

Article

Influence of As-N Interstitial Complexes on Strain Generated in GaAsN Epilayers Grown by AP-MOVPE

Beata Ściana ^{1,*}, Wojciech Dawidowski ^{1,*} , Damian Radziejewicz ¹, Joanna Jadczyk ² ,
Mari Cruz López-Escalante ³, Victor González de la Cruz ³  and Mercedes Gabás ⁴

- ¹ Faculty of Electronics, Photonics and Microsystems, Wrocław University of Science and Technology, Janiszewskiego 11/17, 50-372 Wrocław, Poland; damian.radziejewicz@pwr.edu.pl
- ² Faculty of Fundamental Problems of Technology, Wrocław University of Science and Technology, Wybrzeże Wyspiańskiego 27, 50-370 Wrocław, Poland; joanna.jadczyk@pwr.edu.pl
- ³ The Nanotech Unit, Departamento de Física Aplicada I, Andalucía Tech, Universidad de Málaga, Campus de Teatinos s/n, 29071 Málaga, Spain; mclopez@uma.es (M.C.L.-E.); vmgonzalezdelacruz@gmail.com (V.G.d.I.C.)
- ⁴ Instituto de Energía Solar, ETSIT—Universidad Politécnica de Madrid, Avda. Complutense 30, 28040 Madrid, Spain; mercedes.gabas@upm.es
- * Correspondence: beata.sciana@pwr.edu.pl (B.Ś.); wojciech.dawidowski@pwr.edu.pl (W.D.);
Tel.: +48-71-320-4950 (B.Ś.); +48-71-320-4940 (W.D.)

Abstract: This work presents an investigation of the fully strained GaAsN/GaAs heterostructures obtained by atmospheric pressure metalorganic vapor phase epitaxy, focusing on the analysis of the strain generated in the GaAsN epilayers and its correlation with the formation of split interstitial complexes (N-As)_{As}. We analyzed strained GaAsN epilayers with nitrogen contents and thicknesses varying from 0.93 to 1.81% and 65 to 130 nm, respectively. The composition and thickness were determined by high resolution X-ray diffraction, and the strain was determined by Raman spectroscopy, while the N-bonding configurations were determined by X-ray photoelectron spectroscopy. We found that the strain generated in the GaAsN epilayers is mainly caused by a lattice mismatch with the GaAs substrate. This macroscopic strain is independent of the amount of (N-As)_{As} interstitial defects, while the local strain, induced by an alloying effect, tends to decrease with an increasing ratio of (N-As)_{As} interstitial defects to substitutional nitrogen atoms incorporated into an arsenic sublattice—N_{As}. Here, we show experimentally, for the first time, a correlation between the strain in the GaAsN epilayers, caused by an alloying effect determined by Raman spectroscopy, and the (N-As)_{As}/N_{As} ratio estimated by the XPS method. We found out that the (N-As)_{As} interstitials compensate the local strain resulting from the presence of N in the GaAs matrix, if their amount does not exceed ~65% of the substitutional introduced nitrogen N_{As}.

Keywords: III-V semiconductors; dilute nitrides; AP-MOVPE; nitrogen interstitial complexes; HRXRD; XPS; Raman spectroscopy



Citation: Ściana, B.; Dawidowski, W.; Radziejewicz, D.; Jadczyk, J.; López-Escalante, M.C.; González de la Cruz, V.; Gabás, M. Influence of As-N Interstitial Complexes on Strain Generated in GaAsN Epilayers Grown by AP-MOVPE. *Energies* **2022**, *15*, 3036. <https://doi.org/10.3390/en15093036>

Academic Editors: Yong Shuai and Bachirou Guene Lougou

Received: 9 March 2022

Accepted: 18 April 2022

Published: 21 April 2022

Publisher's Note: MDPI stays neutral with regard to jurisdictional claims in published maps and institutional affiliations.



Copyright: © 2022 by the authors. Licensee MDPI, Basel, Switzerland. This article is an open access article distributed under the terms and conditions of the Creative Commons Attribution (CC BY) license (<https://creativecommons.org/licenses/by/4.0/>).

1. Introduction

Dilute nitride III-V-N alloys, such as arsenides and phosphides with an addition of a small amount of nitrogen, are very attractive semiconductor materials for many novel applications. These semiconductor compounds are highly mismatched alloys (HMAs). This means that a small incorporation of N into typical III-V isovalent alloys results in a strong band restructuring due to the large atomic radius difference between N and As (P) and the high electronegativity of N. This leads to a strong interaction between the localized states produced by N and the extended energy states of the matrix materials and, finally, to an anomalous large band gap reduction [1–5]. In spite of these fundamental issues, these materials are very promising for IR optoelectronics based on GaAs, Ge and Si substrates. For example, quaternary InGaAsN alloys grown compressively strained on GaAs substrate can be used in telecom lasers [6–8], while the same materials or GaAsSbN alloys, lattice

matched to GaAs or Ge substrates with 1 eV bandgap, are very attractive for efficient multijunction solar cells [9–11]. GaNAsP quaternary alloys grown pseudomorphically on Si substrate are very promising for realizing lasers and other photonic devices using this typical microelectronic substrate [12,13]. Alternatively, the technology of dilute nitrides is very difficult and challenging for growers. They require lower growth temperatures than those typical for III-V compounds, in order to avoid a phase segregation, but high enough for a good crystalline quality. As was mentioned earlier, the incorporation of nitrogen into the group V sublattice causes a big impact on the bandgap, and the properties of the dilute nitrides strongly differ from the conventional III-V alloys. In the classical isovalent alloys, a smaller lattice constant increases the band gap, while the mixing of GaAs with a few molar percent of GaN results in a huge reduction of the GaAsN bandgap, due to the smaller covalent radius and large electronegativity of N atoms in comparison to Ga and As. Additionally, it is well known that III-V semiconductor compounds with a cubic zinc-blende crystalline structure become metastable if atoms with a significantly smaller or larger covalent radius than the matrix atoms are alloyed [14]. Technology development using these metastable materials is very difficult because they only can be grown at specific conditions. According to the Hume–Rothery rules [14], in the case of substitutional solid solutions of metals and metallic alloys, a good or complete solubility can be achieved when the solute and the solvent have: a similar crystal structure, an atomic size difference of less than 15%, a small electronegativity difference and the same valency (for a complete solubility). The last rule related to valency is not an issue for the substitutional III-V semiconductor compounds. Other requirements are not fulfilled for the considered dilute nitrides when we mix arsenides and phosphides (Ga, In) (As, P), crystallizing in the cubic zinc-blende structure, with nitrides (Ga, In)N that have the hexagonal wurtzite structure, and the atomic radius and electronegativity differences between nitrogen and the other group V atoms (As, P) are about 30% (Table 1) [1].

Table 1. Characteristic properties of group-V elements [1]. Adapted with permission from [1]. Copyright 2015, Elsevier.

Element	Covalent Radius (pm)	Lattice Constant Ga-Compound (nm)	Electronegativity
N	75	0.452	3.04
P	106	0.54505	2.19
As	119	0.565325	2.18
Sb	138	0.609593	2.05
Bi	146	0.637 (theory)	2.02

These properties' discrepancies cause instability or metastability of certain compositions and local strain introduced into the matrix crystal (the lattice relaxation around N atoms). In the case of the GaAsN ternary alloys considered in this paper, the local static atomic displacements of Ga atoms from their virtual average lattice position is significant (Figure 1) and amounts to 14.3% of the Ga-As bond length [1]. Additionally, in the case of heteroepitaxial structures, we have to take into account a dependence of the solubility on a misfit strain caused by the lattice mismatch between the epilayer and the substrate, which is omitted by Hume–Rothery rules. A significantly larger incorporation of N in the GaAsN epilayers grown on GaP substrate is reported, as compared to the GaAs substrate, because of a strain effect. In the case of the GaP substrate N incorporation in the GaAsN epilayers, an amount below 17% reduces the compressive strain, whereas the N incorporation in the GaAs grown on the GaAs substrate increases the tensile strain of the grown epilayer [1].

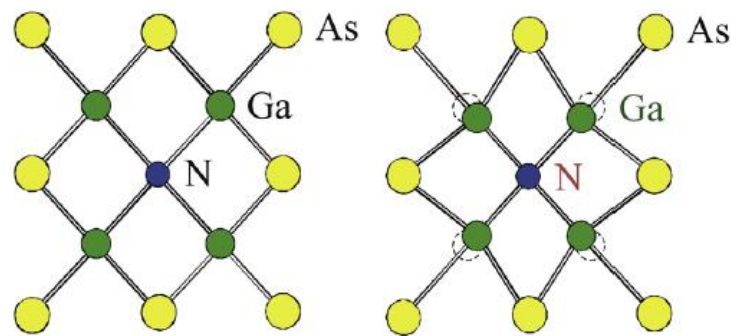


Figure 1. The local static atomic displacements of Ga atoms from their virtual average lattice position introduced by a N atom [1]. Reprinted with permission from [1]. Copyright 2015, Elsevier.

Therefore, the solubility of N in III-V semiconductors can be increased if the N incorporation reduces the macroscopic strain introduced in the growing epilayer. In the case of GaAsN, the strain introduced by the N atoms occupying predominantly the As sublattice N_{As} , that is the substitutional N atoms, can be lowered by the formation of energetically preferred split interstitial N complexes, such as $(N-As)_{As}$ and $(N-N)_{As}$ [15–19], as shown in Figure 2.

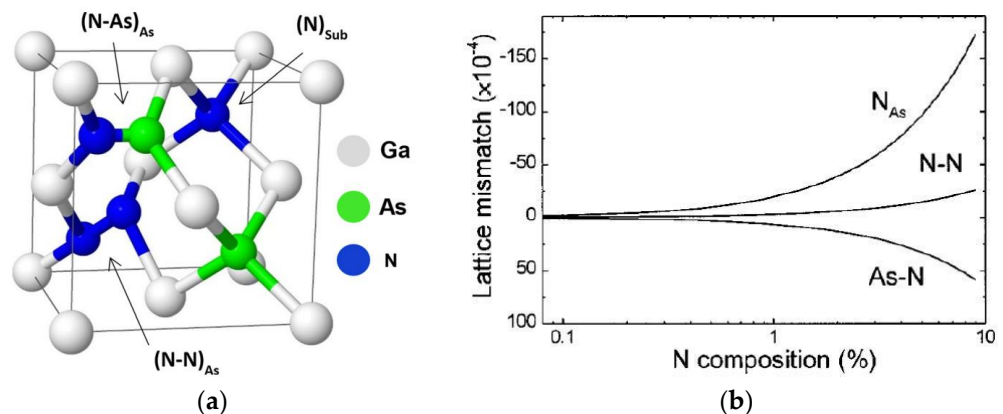


Figure 2. Nitrogen related defects in GaAsN: (a) split interstitial N complexes $(N-As)_{As}$ and $(N-N)_{As}$ [18]; (b) lattice mismatches between GaAsN and GaAs caused by substitutional nitrogen N_{As} , complexes $(N-N)_{As}$ and $(N-As)_{As}$ for different N content [17]. Reprinted with permission from [17,18]. Copyright 2015, 2001, AIP Publishing.

The $(N-As)_{As}$ complex induces a compressive strain, while the $(N-N)_{As}$ defects introduce less tensile strain in comparison to the substitutional nitrogen N_{As} [17], which helps to decrease the local strain and lattice distortion around the N atoms. Conversely, the presence of these interstitial N atoms reduces electron (hole) mobility and non-radiative recombination time, leading to poor device performance, especially in heterojunction bipolar transistors, solar cells and light emitters [20–23]. For this reason, an understanding of the impact of N-related interstitials on the strain and optoelectronic properties of GaAsN alloys is crucial for the improvement of device technology involving these III-V alloys. In this work, we focused on the analysis of the strain generated in the GaAsN epilayers and its correlation with the formation of split interstitial complexes $(N-As)_{As}$. The research was based on the measurements of fully strained GaAsN epilayers by means of high-resolution X-ray diffraction (HRXRD), Raman spectroscopy and X-ray photoelectron spectroscopy (XPS).

2. Experimental Details

The investigated GaAsN/GaAs heterostructures were grown by atmospheric pressure metalorganic vapor phase epitaxy (AP-MOVPE) using the AIX 200 R&D horizontal reactor on a (100)-oriented GaAs substrates. Trimethylgallium TMGa ($\text{Ga}(\text{CH}_3)_3$), tertiarybutylhydrazine TBHy ($(\text{C}_4\text{H}_9)\text{HN}_2\text{H}_2$) and arsine AsH_3 (10% mixture in H_2) were used as growth precursors. The epitaxial structures consist of a 450-nm-thick undoped UD-GaAs buffer followed by undoped UD-GaAsN epilayers. The GaAs buffer was deposited at 670 °C with the flow rates of TMGa and AsH_3 , 19.65 $\mu\text{mol}/\text{min}$ and 1339.29 $\mu\text{mol}/\text{min}$, respectively, providing a V/III molar ratio of 68.16. The GaAsN epilayers were grown at the following constant growth parameters: the TMGa flow rate of 13.76 $\mu\text{mol}/\text{min}$ and the AsH_3 and TBHy flow rates of 223.21 $\mu\text{mol}/\text{min}$ and 601.92 $\mu\text{mol}/\text{min}$, respectively, providing a V/III molar ratio of 59.97. For the GaAsN layers, the only variable parameters were the growth temperature T_g (changed from 565 to 605 °C) and the deposition time τ in the case of the thinnest layer (sample N119). We anticipate here that the thickness d and nitrogen content N of the GaAsN epilayers correlated with the growth temperature T_g and deposition time τ for six investigated samples, which are listed in Table 2.

Table 2. The growth temperature T_g , deposition time τ , nitrogen content N and thickness d of GaAsN epilayers included in six investigated samples.

Sample	T_g (°C)	τ (min)	N (%)	d (nm)
N123	565	20	1.58	100
N120	575	20	1.81	130
N119	585	10	0.93	65
N124	585	20	1.24	102
N121	595	20	1.51	126
N122	605	20	1.39	97

The structural properties, as well as the thickness and composition of GaAsN (Table 2), were examined using HRXRD, (MRD High Resolution X-ray Diffractometer). Raman measurements for strain detection were carried out at room temperature. We used the micro-Raman spectrometer (Renishaw inVia Raman Microscope) in a backscattering configuration with excitation provided by a 633 nm line of a diode-pumped solid-state laser. The diameter of the excitation spot was equal to $\sim 1.5 \mu\text{m}$, and the spectral resolution was 1 cm^{-1} . The system was equipped with a single-pass spectrometer with a grating of 1800 grooves mm^{-1} and a Peltier-cooled CCD array. The power was kept on the order of 250 μW . The N-bonding configurations were studied using X-ray photoelectron spectroscopy. The XPS spectra of the investigated samples were recorded using an X-ray photoelectron spectrometer (Physical Electronics, Inc., model PHI5700, Chanhassen, MN, USA) with a 300 W, Mg $K\alpha$ (1253.6 eV) excitation source, at a fixed voltage of 15 kV, and the vacuum pressure reaches 10^{-9} Torr in the XPS analysis chamber. The spatial resolution and the spot size are defined by the analyser aperture, which is 720 μm in diameter. Core level deconvolution in the several peak components has been made using the commercial CasaXPS software UNIFIT 2009 [24].

3. Results and Discussion

3.1. High Resolution X-ray Diffraction Measurements

Diffraction curves measured for (004) reflection indicated a good structural quality of all samples, as is noted in the GaAsN reflection peak and the presence of Pendellösung fringes in the rocking curves (Figure 3a). The reciprocal space maps (RSMs) recorded for the (115) asymmetrical reflection confirmed that all the structures were fully strained. The exemplary RSM for the sample N120 is shown in Figure 3b.

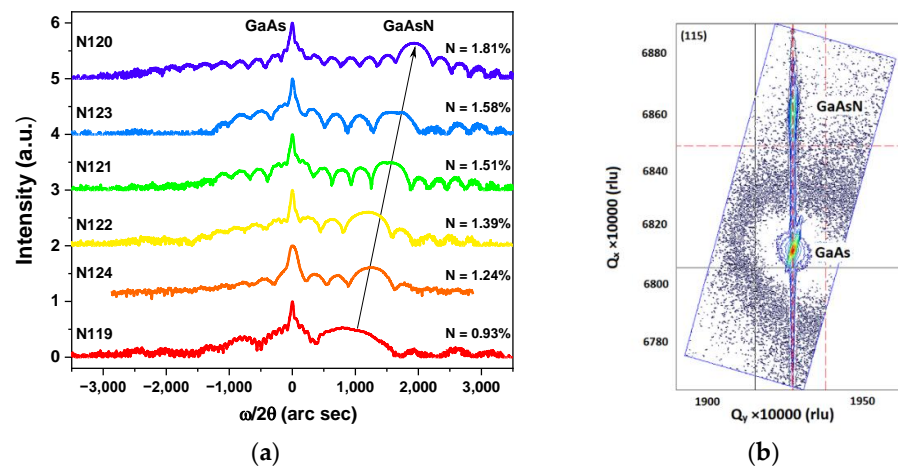


Figure 3. High resolution X-ray diffraction results: (a) the diffraction curves of all investigated heterostructures measured for (004) reflection; (b) the reciprocal space map for the (115) asymmetrical reflection of the sample N120 ($N = 1.81\%$, $d = 130$ nm).

3.2. Raman Measurements and Average Strain Determination

Raman spectroscopy is a sensitive method for studying the local structure of impurity incorporation and deviations from a long-range order induced by the presence of guest atoms. Therefore, it is a powerful technique for detecting the strain introduced into the crystalline structure of different semiconductor materials that results in a frequency shift of the lattice modes. The sensitivity of phonon frequencies to the strain state can be exploited by the phonon deformation potentials (PDP) in bulk materials, epilayers and heterostructures [25]. In our case, the pseudomorphic growth of GaAsN on GaAs increases a biaxial tensile strain in the layer. The average in-plane strain can be well reproduced by the frequency variation of the longitudinal optical mode (ω^{LO}) with respect to the unstrained material. The compressive/tensile nature of the strain manifests by increasing/decreasing frequencies, even on a microscopic (local) scale [26,27]. The main goal of this study was to determine a frequency shift of the GaAs-like longitudinal-optical phonon (GaAs-like LO) in the Raman spectra recorded for the investigated GaAsN epilayers, which could be attributed to the local and macroscopic strain caused by the alloying and lattice mismatch effects, respectively. This knowledge makes it possible to estimate which effect is dominant and to correlate the GaAs-like LO mode frequency shift with the presence of the split interstitial complexes $(N-As)_{As}$, which will be described in the next section devoted to XPS measurements. The measured Raman spectra of the investigated GaAsN/GaAs heterostructures are presented in Figure 4.

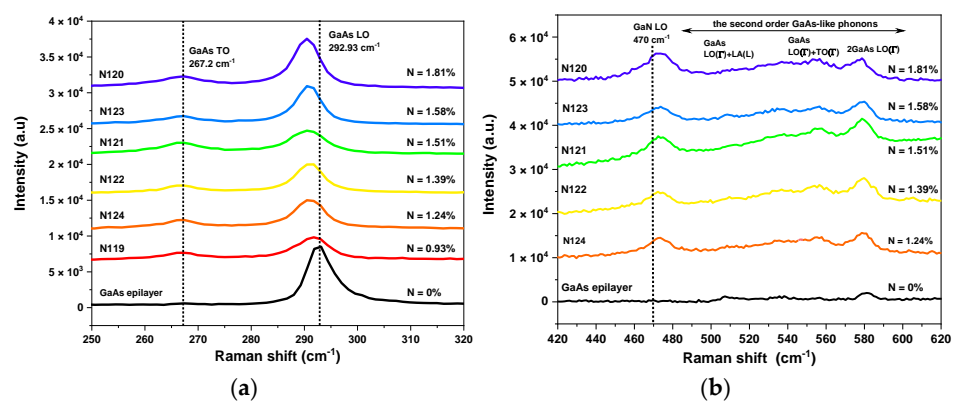


Figure 4. The Raman spectra of the investigated GaAsN/GaAs heterostructures recorded in the spectral range of: (a) the first order GaAs-like modes; (b) the first order GaN-like and the second order GaAs-like phonons.

Figure 4a shows the spectral range of the first order GaAs-like phonons, while Figure 4b covers the spectral range of both the first order GaN-like and the second order GaAs-like phonon modes. It is clearly observed that the red shift of the GaAs-like LO phonon and the blue shift of the GaN-like LO phonon as N content increases, while the GaAs-like TO mode frequency is practically independent of the GaAsN composition. This phonon mode's behavior confirms that the GaAsN epilayers are fully strained (the in-plane lattice constant is the same as GaAs), and the biaxial strain affects only the LO phonon frequency. Based on the measured GaAs-like LO phonon frequency $\omega(N)$, the value of the bulk equivalent frequency $\omega_0(N)$, related to the unstrained (bulk) GaAsN, was calculated using following equation [28,29]:

$$\omega(N) \approx \omega_0(N) \left(1 + \frac{\lambda}{2} \right) \quad (1)$$

where λ is the eigenvalue of Anastassakis' [30] equation, and, for the LO phonon measured from (100) oriented faces, is given by [28,29]:

$$\lambda \approx K_{11}\varepsilon_{zz} + 2K_{12}\varepsilon_{xx} \quad (2)$$

where K_{11} and K_{12} are the phonon deformation potentials, and ε_{xx} and ε_{zz} are the strains in the x (in-plane) and perpendicular z directions, respectively. Assuming that the phonon deformation constants of GaAsN for an N content smaller than 3% are nearly the same as those of GaAs, and applying Vegard's law and HRXRD results for calculation of the ε_{xx} and ε_{zz} strain components, the value of $\omega_0(N)$ was obtained for each investigated sample, as shown in Figure 5a. More details about the applied method and the strain measurements using Raman spectroscopy are described in [28–31]. The calculated values of $\omega_0(N)$ allowed for estimation of the GaAs-like LO frequency shift caused by the lattice mismatch $\omega_{LM} = \omega(N) - \omega_0(N)$ and, thus, for determination of the red shift component related to the alloying effect ω_{AE} . The dependence of the GaAs-like LO frequency shift in the N content of the investigated GaAsN epilayers, with a separate influence of the strain induced by a lattice mismatch and alloying effects, is presented in Figure 5b. The value of the GaAs-like LO frequency for GaAs $\omega(0) = 292.93 \text{ cm}^{-1}$ was determined from the Raman spectrum of the GaAs epitaxial layer.

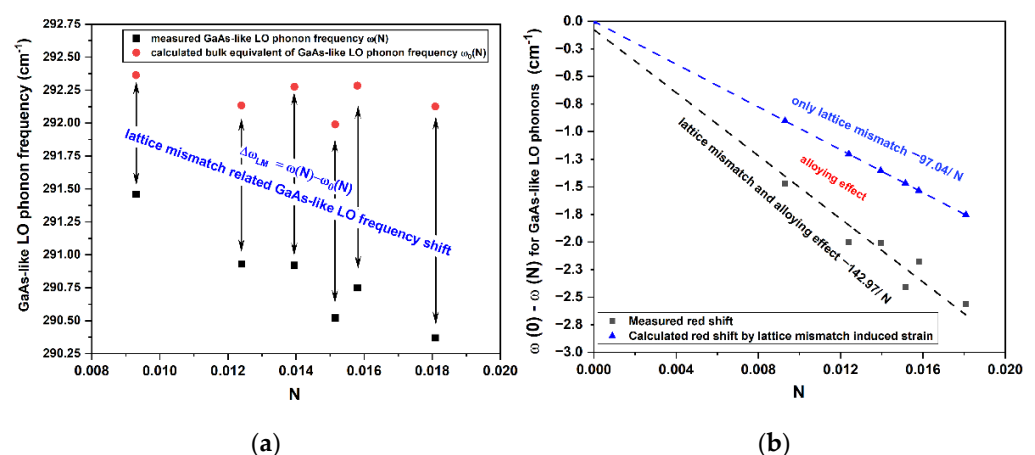


Figure 5. Determined from Raman spectra, two dependencies on N content: (a) GaAs-like LO frequencies of strained GaAsN epilayers (black squares) and calculated bulk GaAsN equivalent frequencies (red circles); (b) the experimental redshift of the GaAs-like LO phonons frequencies (black squares) with the estimated influence of strain induced by a lattice mismatch (blue triangles).

A linear fit of the data obtained from the Raman spectra results in a total shift of the GaAs-like LO phonons $-143 \pm 10 \text{ cm}^{-1}/N$ with a significant contribution of the lattice mismatch induced strain shift $-97 \text{ cm}^{-1}/N$. The additional minor redshift component may

be related to the alloying effect. These values are comparable with the data obtained by T. Prokofyeva et al. in [32] ($-136 \pm 10 \text{ cm}^{-1}/\text{N}$, $-96 \text{ cm}^{-1}/\text{N}$, respectively) for pseudomorphic GaAsN epilayers grown on (001) GaAs substrates with an N content $\leq 3\%$. This confirms the significant impact of a lattice mismatch-related strain on the frequency red shift of GaAs-like LO phonons observed in the Raman spectra of strained GaAsN epilayers. As was mentioned earlier, the $(\text{N-As})_{\text{As}}$ interstitial complexes induce compressive strain in the GaAsN epilayers, which decreases the tensile strain caused by substitutional nitrogen N_{As} . We expect that the presence of these complexes in the GaAsN epilayers will reduce the strain-induced Raman frequency shift of GaAs-like LO phonons. To check this assumption, we used the XPS technique for identification of the possible N-bonding configurations in the investigated GaAsN/GaAs heterostructures.

3.3. XPS Spectra Analysis

X-ray photoelectron spectroscopy is one of the most convenient methods for determination of the N-bonding configurations in GaAsN and InGaAsN epilayers [33–38]. The N 1s core level spectra have been carefully studied for all investigated samples after Ar^+ etching (9 min, acceleration voltage 1–4 kV) of a few nm of the surface GaAsN epilayer, in order to remove the oxygen and carbon contaminations. The exemplary N 1s core level deconvolution spectra corresponding to the samples N122 and N123, grown at the highest (605 °C) and the lowest (565 °C) temperatures, are presented in Figure 6.

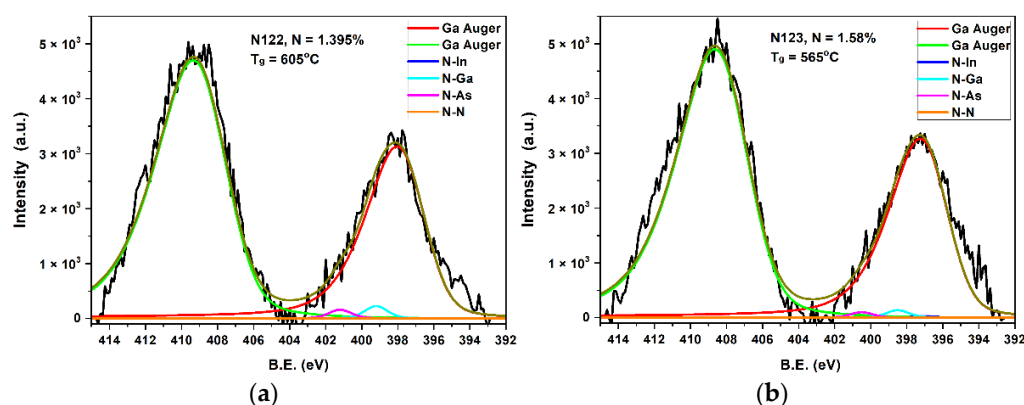


Figure 6. The N 1s core level deconvolution spectra of GaAsN/GaAs heterostructures grown: (a) at the highest and (b) lowest temperatures.

The analysis of the obtained spectra was problematic because of a very intense signal related to the Ga Auger transition overlapping the N1s core level signal observed for all investigated samples. Due to these difficulties, in the deconvolution of the N 1s core level, only three components were identified: N-In (397 eV), N-Ga (398.5 eV) and N-As (400.5 eV) bonds. The contribution related to N-N bonds (402–403 eV) [36,39–41] lies in the binding energy region, where the two Ga Auger transition peaks meet, which makes it impossible to confirm the presence of this interstitial defect. According to a comparison between the N119 and N124 samples, a higher deposition time favors the formation of N-As bonds. Also, very high or low growth temperatures (the N122 and N123 samples, respectively), seem to promote the formation of such interstitial defects. Based on the analysis of N 1s core level deconvolution spectra, the ratio between N-As bonds, corresponding to $(\text{N-As})_{\text{As}}$ interstitial defects, and N-III bonds (N linked to Ga and In) related to N atoms incorporated into the As sublattice N_{As} , was calculated ($\text{N-As}/\text{N-III}$). The obtained values of the $\text{N-As}/\text{N-III}$ ratios are listed in Table 3 and compared with the strain-induced Raman frequency shift of GaAs-like LO phonons caused by the lattice mismatch ω_{LM} and alloying effect ω_{AE} .

Table 3. The ratio of $N\text{-As}/N\text{-III}$, GaAs-like LO frequencies of: GaAs epilayer $\omega(0)$, strained GaAsN epilayer $\omega(N)$, bulk GaAsN $\omega_0(N)$ and Raman frequency shift of GaAs-like LO phonons caused by the lattice mismatch ω_{LM} and alloying effect ω_{AE} determined for all investigated GaAsN/GaAs heterostructures. Red and blue colours represent the calculated values depicted in Figures 7a and 7b, respectively.

Sample	N (%)	$N\text{-As}/N\text{-III}$	$\omega(0)$ (cm^{-1})	$\omega(N)$ (cm^{-1})	$\omega_0(N)$ (cm^{-1})	$\Delta\omega_{AE}$ $\omega_0(N)-\omega(0)$ (cm^{-1})	$\Delta\omega_{LM}$ $\omega(N)-\omega_0(N)$ (cm^{-1})
N121	1.51	0	292.93	290.52	291.99	-0.94	-1.47
N120	1.81	0.408		290.37	292.13	-0.81	-1.75
N119	0.93	0.538		291.46	292.36	-0.57	-0.90
N123	1.58	0.613		290.75	292.28	-0.65	-1.53
N122	1.39	0.724		290.92	292.27	-0.66	-1.35
N124	1.24	1.083		290.93	292.13	-0.80	-1.20

Based on the data included in Table 3, the dependences of the Raman frequency shift of the GaAs-like LO phonons, caused by the strain and alloying effects on the $N\text{-As}/N\text{-III}$ ratio (calculated from XPS spectra), is presented in Figure 7. The dependence in Figure 7a shows the distinct influence of the $N\text{-As}/N\text{-III}$ ratio on the local strain, caused by the alloying effect. It is especially visible when we compare the sample N121 (absence of N-As defects, $N = 1.51\%$) with the samples N123 and N120, which have comparable ($N = 1.58\%$) and the highest ($N = 1.81\%$) nitrogen concentrations, respectively. In both cases, the GaAs-like LO phonon redshift is greater for the sample N121.

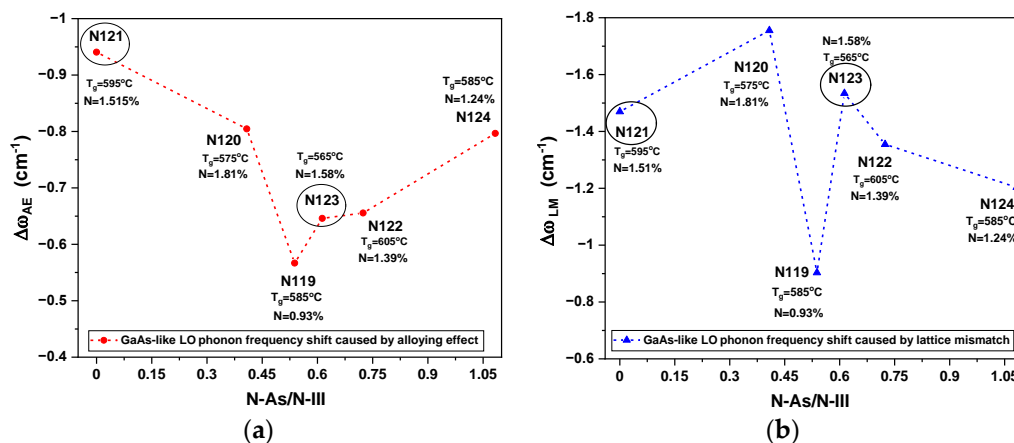


Figure 7. The dependences of GaAs-like LO phonon shift (determined from Raman spectra) caused by the alloying (a) and the strain (b) effects on the $N\text{-As}/N\text{-III}$ ratio (calculated from XPS spectra) for investigated GaAsN/GaAs heterostructures.

That is, the presence of $(N\text{-As})_{As}$ complexes in the N123 and N120 samples compensates partially the tensile strain induced by N incorporation into the GaAs lattice. The visible increase of the Raman shift for $N\text{-As}/N\text{-III} > 0.65$ in the samples with lower N contents (N122 and N124) is probably connected to an increase in the local strain, caused by a large contribution of N-As defects in comparison to N-Ga bonds, which creates the crystalline structure of the GaAsN epilayer. The relation presented in Figure 7b indicates that the $N\text{-As}/N\text{-III}$ ratio has no visible impact on the macroscopic strain caused by a lattice mismatch of GaAsN to GaAs. In this case, the strain-induced GaAs-like LO phonon shift increases with the N content, independent of the value of the $N\text{-As}/N\text{-III}$ ratio. The lowest value of the GaAs-like LO phonon redshift was obtained for the sample N119. In this

GaAsN/GaAs heterostructure, there is the least strain caused by both the lattice mismatch and alloying effects, which is directly connected with the lowest N content of 0.93%.

4. Conclusions

This work presents an investigation of the GaAsN/GaAs heterostructures grown by AP-MOVPE and focuses on the strain generated in as-grown GaAsN epilayers, as well as its correlation with the formation of split interstitial complexes (N-As)_{As}. Based on the GaAs-like LO phonon frequency $\omega(N)$, determined from the measured Raman spectra, the value of bulk equivalent frequency $\omega_0(N)$ related to the unstrained GaAsN was calculated. This allowed for estimation of the influence of the macroscopic and local strain, resulting from the lattice mismatch and alloying effect, respectively, on the LO phonon frequency redshift. Thanks to this, it was possible to separately correlate these strain components with the ratio of the (N-As)_{As} interstitial defects to the N atoms incorporated into the As sublattice, N_{As} , calculated from XPS spectra ($N-As/N-III$). It was found that (N-As)_{As} interstitial complexes have no significant effect on the macroscopic strain but are able to compensate for the local strain caused by alloying effect, if their amount does not exceed ~65% of the substitutional introduced nitrogen N_{As} . Future research will be extended to post-growth annealed GaAsN epilayers and InGaAsN/GaAs heterostructures.

Author Contributions: Conceptualization, B.Ś.; data curation, B.Ś., M.C.L.-E. and M.G.; investigation, B.Ś., W.D., D.R., J.J., M.C.L.-E., V.G.d.I.C. and M.G.; methodology, B.Ś. and W.D.; project administration, B.Ś.; supervision, B.Ś.; writing—original draft, B.Ś.; writing—review & editing, B.Ś., W.D., J.J. and M.G. All authors have read and agreed to the published version of the manuscript.

Funding: This research received no external funding.

Institutional Review Board Statement: Not applicable.

Informed Consent Statement: Not applicable.

Data Availability Statement: Data are available on request from the corresponding author.

Acknowledgments: This work was co-financed by the Polish National Agency for Academic Exchange under the contract number BPN/BSK/2021/1/00035/U/00001, the Wrocław University of Science and Technology subsidy, the Slovak Research and Development Agency SK-PL-21-0041, the Spanish MCIN/AEI/10.13039/501100011033 and the European Union “NextGenerationEU”/PRTR through the project PDC2021-120748-I00, the Comunidad de Madrid through the project MADRID-PV2 (S2018/EMT-4308), and by the Universidad de Málaga through Plan Propio de la UMA, D5-Ayudas para la constitución de redes temáticas: “Materiales avanzados aplicables a las tecnologías facilitadoras esenciales” D5-2020_09.

Conflicts of Interest: The authors declare no conflict of interest.

References

1. Beyer, A.; Stolz, W.; Volz, K. Metastable cubic zinc-blende III/V semiconductors: Growth and structural characteristics. *Prog. Cryst. Growth Charact. Mater.* **2015**, *61*, 46–62. [[CrossRef](#)]
2. Stringfellow, G. Epitaxial growth of metastable semiconductor alloys. *J. Cryst. Growth* **2021**, *564*, 126065. [[CrossRef](#)]
3. Walukiewicz, W.; Zide, J.M.O. Highly Mismatched Semiconductor Alloys: From Atoms to Devices. *J. Appl. Phys.* **2020**, *127*, 010401. [[CrossRef](#)]
4. Ściana, B.; Radziejewicz, D.; Dawidowski, W.; Biela, K.; Szyszka, A.; Kopaczek, J. Impact of gallium concentration in the gas phase on composition of InGaAsN alloys grown by AP-MOVPE correlated with their structural and optical properties. *J. Mater. Sci. Mater. Electron.* **2019**, *30*, 16216–16225. [[CrossRef](#)]
5. Shan, W.; Yu, K.M.; Walukiewicz, W.; Wu, J.; Ager, J.; Haller, E.E. Band anticrossing in dilute nitrides. *J. Phys. Condens. Matter* **2004**, *16*, S3355–S3372. [[CrossRef](#)]
6. Bank, S.R.; Bae, H.; Goddard, L.L.; Yuen, H.B.; Wistey, M.A.; Kudrawiec, R.; Harris, J.S. Recent Progress on 1.55- μ m Dilute-Nitride Lasers. *IEEE J. Quantum Electron.* **2007**, *43*, 773–785. [[CrossRef](#)]
7. Tansu, N.; Yeh, J.-Y.; Mawst, L. High-performance 1200-nm InGaAs and 1300-nm InGaAsN quantum-well lasers by metalorganic chemical vapor deposition. *IEEE J. Sel. Top. Quantum Electron.* **2003**, *9*, 1220–1227. [[CrossRef](#)]
8. Tomic, F.S.; O'Reilly, E.P.; Fehse, R.; Sweeney, S.; Adams, A.; Andreev, A.; Choulis, S.; Hosea, T.J.C.; Riechert, H. Theoretical and experimental analysis of 1.3- μ m InGaAsN/GaAs lasers. *IEEE J. Sel. Top. Quantum Electron.* **2003**, *9*, 1228–1238. [[CrossRef](#)]

9. Polojärvi, V.; Aho, A.; Tukiainen, A.; Raappana, M.; Aho, T.; Schramm, A.; Guina, M. Influence of As/group-III flux ratio on defects formation and photovoltaic performance of GaInNAs solar cells. *Sol. Energy Mater. Sol. Cells* **2016**, *149*, 213–220. [[CrossRef](#)]
10. Dawidowski, W.; Ściana, B.; Zborowska-Lindert, I.; Mikolášek, M.; Kováč, J.; Tlaczala, M. Tunnel junction limited performance of InGaAsN/GaAs tandem solar cell. *Sol. Energy* **2020**, *214*, 632–641. [[CrossRef](#)]
11. Gonzalo, A.; Stanojević, L.; Marrón, D.F.; Guzman, A.; Hierro, A.; Ulloa, J. 1 eV GaAsSbN-based solar cells for efficient multi-junction design: Enhanced solar cell performance upon annealing. *Sol. Energy* **2021**, *221*, 307–313. [[CrossRef](#)]
12. Kunert, B.; Volz, K.; Stolz, W. Properties and Laser Applications of the GaP-Based (GaNAsP)-Material System for Integration to Si Substrates. In *Dilute III-V Nitride Semiconductors and Material Systems. Materials Science*; Erol, A., Ed.; Springer: Berlin/Heidelberg, Germany, 2008; Volume 105. [[CrossRef](#)]
13. Liebich, S.; Zimprich, M.; Beyer, A.; Lange, C.; Franzbach, D.J.; Chatterjee, S.; Hossain, N.; Sweeney, S.; Volz, K.; Kunert, B.; et al. Laser operation of Ga(NAsP) lattice-matched to (001) silicon substrate. *Appl. Phys. Lett.* **2011**, *99*, 071109. [[CrossRef](#)]
14. Hume-Rothery, W.; Smallman, R.W.; Haworth, W.C. *The Structure of Metals and Alloys*; Institute of Metals and the Institution of Metallurgists: London, UK, 1969.
15. Li, J.; Han, X.; Dong, C.; Fan, C. Formation energies of substitutional NAs and split interstitial complexes in dilute GaAsN alloys with different growth orientations. *Appl. Phys. A* **2018**, *124*, 108. [[CrossRef](#)]
16. Zhang, S.B.; Wei, S.-H. Nitrogen Solubility and Induced Defect Complexes in Epitaxial GaAs:N. *Phys. Rev. Lett.* **2001**, *86*, 1789–1792. [[CrossRef](#)] [[PubMed](#)]
17. Li, W.; Pessa, M.; Likonen, J. Lattice parameter in GaNAs epilayers on GaAs: Deviation from Vegard's law. *Appl. Phys. Lett.* **2001**, *78*, 2864–2866. [[CrossRef](#)]
18. Jen, T.; Vardar, G.; Wang, Y.Q.; Goldman, R.S. Identifying the dominant interstitial complex in dilute GaAsN alloys. *Appl. Phys. Lett.* **2015**, *107*, 221904. [[CrossRef](#)]
19. Querales-Flores, J.D.; Ventura, C.I.; Fuhr, J.D. Effect of N interstitial complexes on the electronic properties of GaAs_{1-x}N_x alloys from first principles. *Phys. Rev. Mater.* **2019**, *3*, 024602. [[CrossRef](#)]
20. Kosa, A.; Stuchlikova, L.; Harmatha, L.; Mikolasek, M.; Kovac, J.; Ściana, B.; Dawidowski, W.; Radziejewicz, D.; Tlaczala, M. Defect distribution in InGaAsN/GaAs multilayer solar cells. *Sol. Energy* **2016**, *132*, 587–590. [[CrossRef](#)]
21. Tan, L.J.J.; Soong, W.M.; David, J.P.R.; Ng, J.S. Dark Current Mechanism in Bulk GaInNAs Lattice Matched to GaAs. *IEEE Trans. Electron Devices* **2010**, *58*, 103–106. [[CrossRef](#)]
22. Loke, W.K.; Yoon, S.F.; Wicaksono, S.; Tan, K.H.; Lew, K.L. Defect-induced trap-assisted tunneling current in GaInNAs grown on GaAs substrate. *J. Appl. Phys.* **2007**, *102*, 054501. [[CrossRef](#)]
23. Dawidowski, W.; Ściana, B.; Bielak, K.; Mikolášek, M.; Drobný, J.; Serafińczuk, J.; Lombardero, I.; Radziejewicz, D.; Kijaszek, W.; Kósa, A.; et al. Analysis of Current Transport Mechanism in AP-MOVPE Grown GaAsN p-i-n Solar Cell. *Energies* **2021**, *14*, 4651. [[CrossRef](#)]
24. Unitfit for Windows, The Art of Peak Fit. Available online: <https://www.unifit-software.de/publications.html> (accessed on 1 March 2022).
25. Giulotto, E.; Geddo, M. Micro-Raman Mapping of the Strain Field in GaAsN/GaAsN:H Planar Heterostructures: A Brief Review and Recent Evolution. *Appl. Sci.* **2019**, *9*, 4864. [[CrossRef](#)]
26. Shin, H.K.; Lockwood, D.J.; Lacelle, C.; Poole, P.J. Phonons in strained In_{1-x}Ga_xAs/InP epilayers. *J. Appl. Phys.* **2000**, *88*, 6423–6428. [[CrossRef](#)]
27. Bellani, V.; Bocchi, C.; Ciabattoni, T.; Franchi, S.; Frigeri, P.; Galinetto, P.; Geddo, M.; Germini, F.; Guizzetti, G.; Nasi, L.; et al. Residual strain measurements in InGaAs metamorphic buffer layers on GaAs. *Eur. Phys. J. B* **2007**, *56*, 217–222. [[CrossRef](#)]
28. Burns, G.; Wie, C.R.; Dacol, F.H.; Pettit, G.D.; Woodall, J.M. Phonon shifts and strains in strain-layered (Ga_{1-x}In_x)As. *Appl. Phys. Lett.* **1987**, *51*, 1919–1921. [[CrossRef](#)]
29. Jainy, S.C.; Willander, M.; Maes, H. Stresses and strains in epilayers, stripes and quantum structures of III-V compound semiconductors. *Semicond. Sci. Technol.* **1996**, *11*, 641–671. [[CrossRef](#)]
30. Anastassakis, E. Stress measurements using Raman scattering. In Proceedings of the 19th European Solid State Device Research Conference, Berlin, Germany, 11–14 September 1989; Volume 90-11, pp. 298–326.
31. Giulotto, E.; Geddo, M.; Patrini, M.; Guizzetti, G.; Sharma, M.S.; Capizzi, M.; Polimeni, A.; Pettinari, G.; Rubini, S.; Felici, M. Strain related relaxation of the GaAs-like Raman mode selection rules in hydrogenated GaAs_{1-x}N_x layers. *J. Appl. Phys.* **2019**, *125*, 175701. [[CrossRef](#)]
32. Prokofyeva, T.; Sauncy, T.; Seon, M.; Holtz, M.; Qiu, Y.; Nikishin, S.; Temkin, H. Raman studies of nitrogen incorporation in GaAs_{1-x}N_x. *Appl. Phys. Lett.* **1998**, *73*, 1409–1411. [[CrossRef](#)]
33. Chang, W.; Lin, J.; Zhou, W.; Chua, S.J.; Feng, Z.C. Photoluminescence and photoelectron spectroscopic analysis of InGaAsN grown by metalorganic chemical vapor deposition. *Appl. Phys. Lett.* **2001**, *79*, 4497–4499. [[CrossRef](#)]
34. Veal, T.D.; Mahboob, I.; Piper, L.F.J.; Ashley, T.; Hopkinson, M.; McConville, C.F. Electron spectroscopy of dilute nitrides. *J. Phys. Condens. Matter* **2004**, *16*, S3201–S3214. [[CrossRef](#)]
35. Lay, T.S.; Kuo, W.T.; Chen, L.P.; Lai, Y.H.; Hung, W.H.; Wang, J.S.; Chi, J.Y.; Shih, D.K.; Lin, H.H. Probing the electronic structures of III-V-nitride semiconductors by x-ray photoelectron spectroscopy. *J. Vac. Sci. Technol. B* **2004**, *22*, 1491–1494. [[CrossRef](#)]

36. López-Escalante, M.; Ściana, B.; Dawidowski, W.; Bielak, K.; Gabás, M. Atomic configurations in AP-MOVPE grown lattice-mismatched InGaAsN films unravelled by X-ray photoelectron spectroscopy combined with bulk and surface characterization techniques. *Appl. Surf. Sci.* **2018**, *433*, 1–9. [[CrossRef](#)]
37. Milanova, M.; Donchev, V.; Kostov, K.L.; Alvarez, D.A.; Terziyska, P.; Avdeev, G.; Valcheva, E.; Kirilov, K.; Georgiev, S. Study of GaAsSb:N bulk layers grown by liquid phase epitaxy for solar cells applications. *Mater. Res. Express* **2019**, *6*, 075521. [[CrossRef](#)]
38. Milanova, M.; Donchev, V.; Kostov, K.L.; Alonso-Álvarez, D.; Valcheva, E.; Kirilov, K.; Asenova, I.; Ivanov, I.G.; Georgiev, S.; Ekins-Daukes, N. Experimental study of the effect of local atomic ordering on the energy band gap of melt grown InGaAsN alloys. *Semicond. Sci. Technol.* **2017**, *32*, 085005. [[CrossRef](#)]
39. Chen, X.; Zhang, D.; Jin, Y.; Li, J.; Teng, J.; Yakovlev, N. Effect of rapid thermal annealing on behavior of nitrogen in GaAsN alloys. *J. Cryst. Growth* **2013**, *362*, 197–201. [[CrossRef](#)]
40. Hecht, J.-D.; Frost, F.; Hirsch, D.; Neumann, H.; Schindler, A.; Preobrajenski, A.B.; Chassé, T. Interstitial nitrogen induced by low-energy ion beam nitridation of AIII–BV semiconductor surfaces. *J. Appl. Phys.* **2001**, *90*, 6066–6069. [[CrossRef](#)]
41. Jin, Y.; Tang, X.; Teng, J.; Zhang, D. Optical properties and bonding behaviors of InSbN alloys grown by metal-organic chemical vapor deposition. *J. Cryst. Growth* **2015**, *416*, 12–16. [[CrossRef](#)]